Longitudinal flightpath predictor design for minimum pilot compensation

G Sachs
Institute of Flight Mechanics and Flight Control, Technische Universität München, Boltzmannstrasse 15, 85747 Garching, Germany

Abstract: Flightpath prediction can substantially enhance the guidance and control capabilities offered by a novel display type that presents guidance information in a three-dimensional format. Based on pilot-centred requirements, a predictor design for longitudinal motion is proposed to achieve minimum pilot compensation for controlling the predictor–aircraft system. Key configuration factors of the pilot–predictor–aircraft system are identified and optimized. The compensatory control issues are verified in a simulation test program.

Keywords: flightpath predictor, perspective flightpath display, manual control, flightpath control, aircraft guidance

NOTATION

C_D	drag coefficient
C_L	lift coefficient
e_{PR}	predictor position error
g	acceleration due to gravity
h	altitude (with $h(s)$ denoting the s-domain variable and $h(t)$ the time-domain variable)
K	gain
M_α	pitching moment due to the angle of attack
M_{δ_e}	pitching moment due to the pitch control input
s	Laplace operator
t	time
T	thrust
$T_{1,2}$	time constants
T_{h_i}	numerator time constant of the altitude-to-pitch control transfer function, $i = 1, 2, 3$
T_{PR}	prediction time
$\overline{T}_{PR}$	prediction time related to centrifugal acceleration
V	speed
$Y_C(s)$	aircraft transfer function
$Y_P(s)$	pilot transfer function
$Y_{PR}(s)$	predictor transfer function
Z_α	vertical force due to the angle of attack
Z_{δ_e}	vertical force due to the pitch control input
γ	flightpath angle (with $\gamma(s)$ denoting the s-domain variable and $\gamma(t)$ the time-domain variable)
$\dot{\gamma}$	flightpath angle rate (with $\dot{\gamma}(s)$ denoting the s-domain variable and $\dot{\gamma}(t)$ the time-domain variable)
Δ	denoting a perturbation, e.g. Δh
δ_e	pitch control deflection
ζ_P	damping ratio of the phugoid
ζ_{SP}	damping ratio of the short period mode
τ_e	effective time delay
ω_C	crossover frequency
ω_P	natural angular frequency of the phugoid
ω_{SP}	natural angular frequency of the short period mode

The MS was received on 2 August 1999 and was accepted after revision for publication on 1 November 1999.

1 INTRODUCTION

A substantial enhancement in the guidance and control of aircraft is possible with a new type of display with predictive capability because it provides the pilot with three-dimensional information of the command and future flightpaths of the aircraft. By contrast, current instrumentation is basically restricted to a planar picture of aircraft position and heading. It necessitates scanning and mental efforts to achieve an adequate level of navigational awareness. The pilot has mentally to reconstruct the spatial and temporal situation of the aircraft from planar displays.

In recent research, significant progress has been achieved in utilizing novel displays presenting a perspective flightpath image and predictive elements [**1**–**10**]. This research consists of new concepts and theoretical investigations as well as simulation experiments and flight tests. The flight test verification included the first landing of an aircraft with a pictorial display presenting three-

dimensional guidance information (synthetic vision) as the only visual information for the pilot [**8**, **9**]. The results achieved up to now show that perspective flightpath displays basically yield an improvement in performance in regard to preciseness of control as well as to reduction in control activity. This improvement can be substantially increased when predictive information is included in the perspective flightpath display.

There are various aspects contributing to the improvements offered by predictive displays which present the information in a way that takes the specific human capabilities in the areas of perception, cognition and control into account. Predictive displays yield an enhancement of control possibilities for the pilot, an improvement in situation awareness and a reduction in scanning effort.

A central issue of a predictive capability is compensatory flightpath control, which is the subject of this paper. Research thus far has placed emphasis on the lateral motion of aircraft and related guidance and control improvements possible with predictive displays, which have been examined in great detail; e.g. recent results are reported in references [**1**], [**3**] to [**5**], [**7**] and [**10**]. By contrast, comparatively little has been reported about the application of perspective flightpath displays to longitudinal motion. It is therefore the purpose of this paper to consider the addressed predictor issues for the longitudinal motion. It will be shown that there are unique properties of longitudinal flightpath control, and new solutions will be presented for the application of predictive flightpath displays.

2 PILOT-CENTRED REQUIREMENTS FOR COMPENSATORY PREDICTOR CONTROL

A predictive flightpath display, which presents the future aircraft position and the command trajectory in a perspective format to the pilot (Fig. 1), offers novel control modes when compared with current cockpit instrumentation. Basic issues concerning control modes and pilot-centred requirements for the application of perspective flightpath displays with a predictive capability are considered in reference [**10**]. An important issue is compensatory control which can be regarded as a primary control task when using a predictor for a perspective flightpath display. The related application to the longitudinal motion will be considered in this paper.

A primary goal of the predictor design is to minimize pilot effort while retaining maximum system performance. From manual control theory it is known that the pilot can adapt his characteristics to compensate for deficiencies of a controlled element [**11**, **12**]. For this purpose, he may develop low-frequency lead or adjust his gain. When low-frequency lead is required, the associated cost is increased pilot time delay, degraded system performance and a degradation in pilot ratings.

To avoid such detrimental effects and achieve best results in terms of performance and workload, the following design requirement for the predictor may be set up:

(a) no low-frequency lead equalization required by the pilot,
(b) pilot loop closure possible over a wide range of gains.

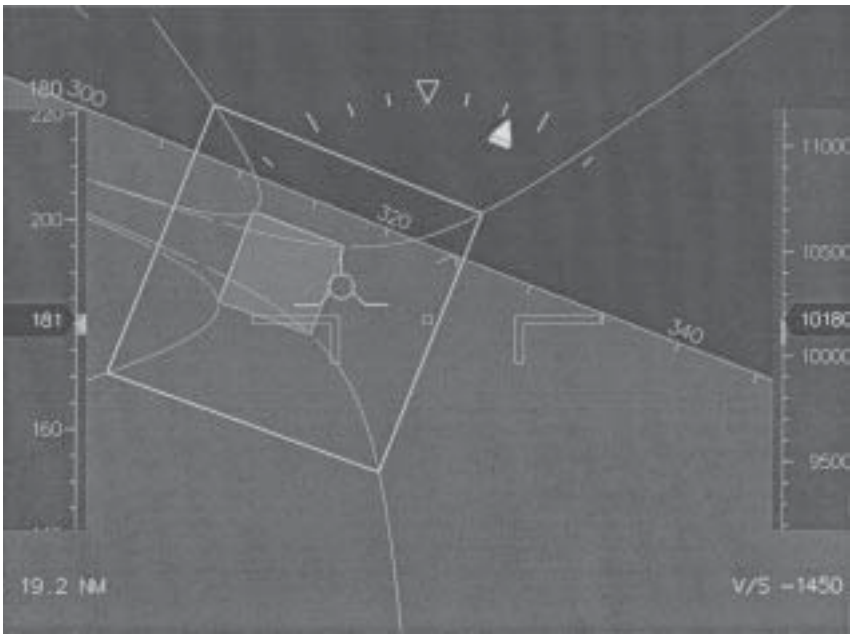

Fig. 1 Perspective flightpath display with a predictor for future aircraft position

This pilot-centred requirement can be met with two predictor candidates yielding the following properties: the effective transfer characteristic of the predictor–aircraft system, $Y_{PR}(s)Y_C(s)$, approximates either a pure gain or a pure integration over an adequately broad region centred around pilot–predictor–aircraft crossover, i.e.

Pure gain

$$Y_{PR}(s)Y_C(s) = K \tag{1}$$

Pure integration

$$Y_{PR}(s)Y_C(s) = \frac{K}{s} \tag{2}$$

Equations (1) and (2) describe desired dynamic characteristics of the predictor–aircraft system as the controlled element. Thus, they can be used as a requirement for designing the predictor to achieve appropriate dynamic behaviour of the closed-loop pilot–predictor–aircraft system.

Also, there are further dynamic requirements of concern:

(a) system stability,
(b) system bandwidth.

3 BASIC PREDICTOR

A perspective flightpath display with a predictor is intended to provide the pilot with three-dimensional information about the command flightpath and the future position of the aircraft. A detailed form of an experimental perspective flightpath display is shown in Fig. 1 which presents the command flightpath in a three-dimensional format (tunnel) and a predictive element (predictor) as well as other, integrated guidance elements to the pilot. A reduced form of a perspective flightpath display depicting the basic elements of predictor and command flightpath is graphically illustrated in Fig. 2. This figure shows that the position of the predictor is referenced to the command flightpath with the use of a specially marked cross-section frame of the tunnel at the prediction time ahead. Determination of the predictor position is based on an estimated continuation of the flightpath for which various estimation models are in use. A promising model featuring a second-order predictor yields a circular continuation of the flightpath [**1**, **3**–**5**, **7**, **10**]. The geometric and kinematic relationships for describing a circular flightpath continuation are shown in Fig. 3, from which it follows that the displacement of the predicted position from the command flightpath at the prediction time T_{PR} ahead may be expressed as

$$\Delta h_{PR}(t) = \Delta h(t) - h_C^*(t) + VT_{PR}\Delta\gamma(t) + V\frac{T_{PR}^2}{2}\Delta\dot{\gamma}(t) \tag{3}$$

where

$$h_{PR}(t) = h(t + T_{PR})$$

The displacement of the predicted position can be described with a combination of quantities of the current aircraft motion, as graphically illustrated with the block diagram and related pathways in Fig. 4. Accordingly, these quantities can be considered to be available from measurements of sensors on board the aircraft. The following relation for the displacement Δh_{PR}, referenced to flightpath angle rate, holds using the Laplace transformation (applied to deviations, with zero initial conditions):

$$\Delta h_{PR}(s) = \left(K_{\dot{\gamma}} + \frac{K_\gamma}{s} + \frac{V}{s^2}\right)\Delta\dot{\gamma}(s) \tag{4}$$

When the gains K_γ and $K_{\dot{\gamma}}$ are selected as

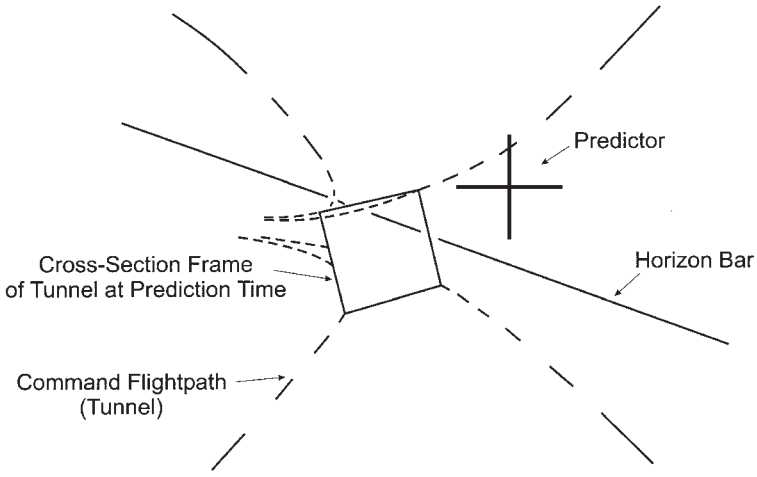

Fig. 2 Basic elements of the perspective flightpath display with a predictor

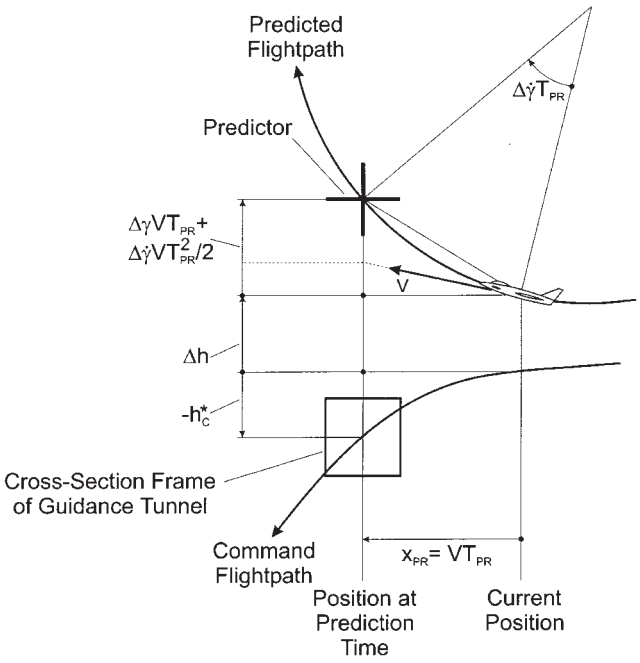

Fig. 3 Displacement of the predictor with circular flightpath continuation

$$K_\gamma = VT_{\mathrm{PR}}, \qquad K_{\dot\gamma} = V\frac{T_{\mathrm{PR}}^2}{2} \tag{5}$$

the displacement $\Delta h_{\mathrm{PR}}(s)$ corresponds to the circular flightpath continuation model, as described by equation (3):

$$\Delta h_{\mathrm{PR}}(s) = V\left(\frac{T_{\mathrm{PR}}^2}{2} + \frac{T_{\mathrm{PR}}}{s} + \frac{1}{s^2}\right)\Delta\dot\gamma(s) \tag{6}$$

The displacement Δh_{PR} is indicated by the predictor symbol in the perspective flightpath display as an error e_{PR} (Fig. 4). The relation between Δh_{PR} and e_{PR} may be expressed as

$$e_{\mathrm{PR}}(s) = K_{\mathrm{PR}}\Delta h_{\mathrm{PR}}(s) \tag{7}$$

With the use of equations (6) and (7), the transfer function between the flightpath angle rate and the error presented by the predictor symbol reads

$$(Y_{\mathrm{PR}})_{\mathrm{circular}} = \frac{e_{\mathrm{PR}}(s)}{\Delta\dot\gamma(s)} = K_{\mathrm{PR}}V\frac{(T_{\mathrm{PR}}^2/2)s^2 + T_{\mathrm{PR}}s + 1}{s^2} \tag{8}$$

This transfer function describes the dynamic characteristics of a predictor with circular flightpath continuation. There are two factors, T_{PR} and K_{PR}, which can be selected for best equalization for the controlled aircraft–predictor element.

The dynamics of the aircraft can be described with the short-term dynamics model characterized by the short period mode with undamped natural frequency and damping ratio ω_{SP} and ζ_{SP}. This is because the short period mode can be considered to be the dominant mode of the augmented vehicle for the frequency region of concern. The corresponding transfer function reads (e.g. according to reference [**13**])

$$Y_{\mathrm{C}} = \frac{\Delta\dot\gamma(s)}{\delta_{\mathrm{e}}(s)} = -\frac{Z_{\delta_{\mathrm{e}}}}{V}\frac{(s+1/T_{h_2})(s+1/T_{h_3})}{s^2 + 2\zeta_{\mathrm{SP}}\omega_{\mathrm{SP}}s + \omega_{\mathrm{SP}}^2} \tag{9a}$$

For the following analytical treatment, the numerator zeros, which are real valued and related to each other according to $1/T_{h_2} \approx -1/T_{h_3} \approx \sqrt{M_\alpha - Z_\alpha M_{\delta_{\mathrm{e}}}/Z_{\delta_{\mathrm{e}}}}$, may be ignored because they are usually larger than ω_{SP} so that there is only a minor effect on the frequency region of pilot–system

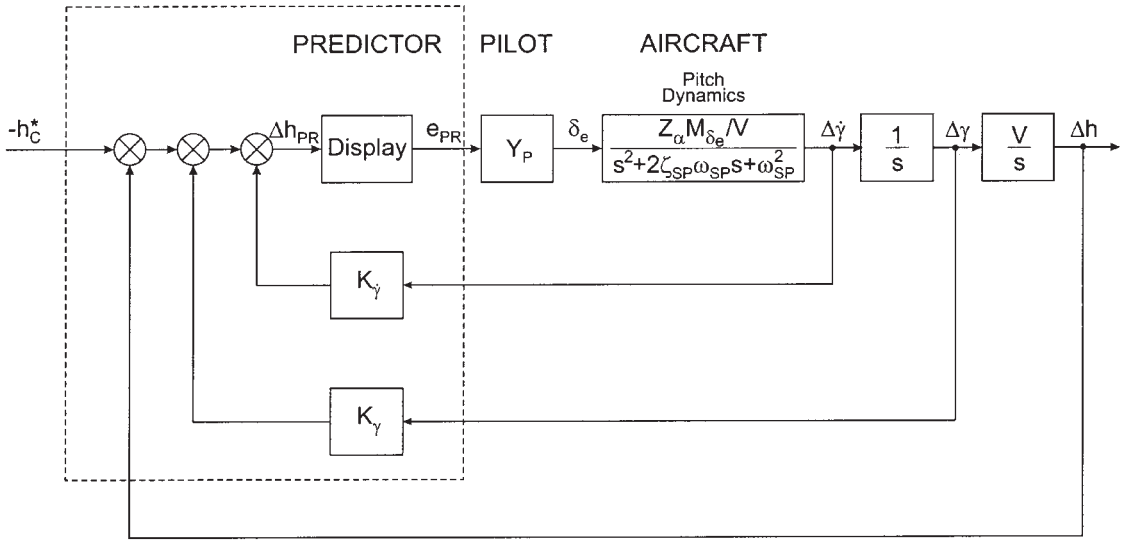

Fig. 4 Block diagram for the predictor

crossover which is of primary concern. Therefore, the aircraft dynamics may be modelled as

$$Y_C = \frac{\Delta\dot{\gamma}(s)}{\delta_e(s)} = -\frac{Z_\alpha M_{\delta_e}/V}{s^2 + 2\zeta_{SP}\omega_{SP}s + \omega_{SP}^2} \tag{9b}$$

Combining equations (8) and (9b) yields the open-loop transfer function of the controlled element (effective predictor to longitudinal control response, without pilot):

$$\left.\frac{e_{PR}(s)}{\delta_e(s)}\right|_{circular} = -K_{PR} Z_\alpha M_{\delta_e} \frac{T_{PR}^2}{2} \frac{s^2 + (2/T_{PR})s + 2/T_{PR}^2}{s^2(s^2 + 2\zeta_{SP}\omega_{SP}s + \omega_{SP}^2)} \tag{10}$$

The zeros of the numerator which may be rewritten as

$$s^2 + 2\zeta_{PR}\omega_{PR}s + \omega_{PR}^2 = s^2 + (2/T_{PR})s + 2/T_{PR}^2 \tag{11}$$

can be described by

$$\omega_{PR} = \frac{\sqrt{2}}{T_{PR}}, \qquad \zeta_{PR} = \frac{1}{\sqrt{2}} \tag{12}$$

The predictor–aircraft transfer characteristics of the basic predictor are illustrated in Fig. 5 which shows a generic Bode plot of the open-loop predictor–aircraft system. For compensatory control, the frequency region of primary concern is the region between ω_{PR} and ω_{SP}, i.e.

$$\omega_{PR} \leqslant \omega \leqslant \omega_{SP}$$

This is because it can be regarded as the region where pilot–system crossover occurs. Figure 5 shows that there is a K characteristic in this frequency region. As a result, the basic predictor with a circular flightpath continuation can be considered a design candidate for the desired controlled element characteristics.

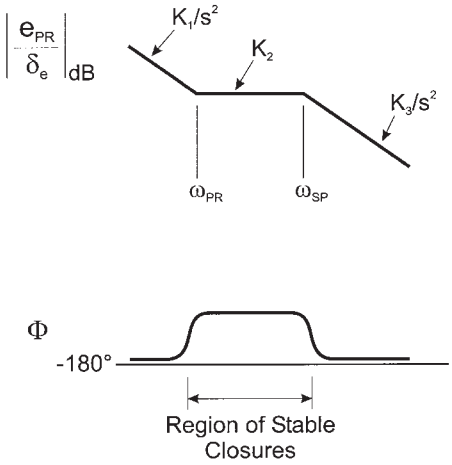

Fig. 5 Asymptotic Bode plot for the predictor–aircraft system (basic predictor with circular flightpath continuation)

4 PREDICTOR EXTENSION: CONTROL RELATED FLIGHTPATH CONTINUATION MODEL

An extension of the predictor concept is introduced in this section in order to achieve a K/s characteristic in the frequency region of pilot–system crossover. Manual control theory shows that an effective controlled element having a K/s characteristic is nearly as good as a pure gain with regard to pilot response and performance. However, the proposed predictor extension has distinct advantages as regards closed-loop properties. Therefore, emphasis will be placed on this predictor candidate in the following sections.

The predictor extension concerns the gains K_γ and $K_{\dot{\gamma}}$ which are now selected independently of each other. With reference to the related pathways in the block diagram of Fig. 4, the independent gain selection can be described in the following form

$$K_\gamma = VT_{PR}, \qquad K_{\dot{\gamma}} = V\frac{\overline{T}_{PR}^2}{2} \tag{13}$$

This selection may be understood as introducing different prediction times for the effects of the flightpath angle, T_{PR}, and the centrifugal acceleration, $\overline{T}_{PR}$, yielding different contributions of $\Delta\gamma$ and $\Delta\dot{\gamma}$ to the predicted trajectory when compared with the above circular flightpath continuation. As a consequence, the predicted flightpath differs from the basic predictor case.

The γ-related time, T_{PR}, is regarded as the prediction time which is considered to describe the time ahead of the predictor position. This understanding is supported by the selection of $\overline{T}_{PR}$ as a significantly smaller quantity (as will be shown later).

It may be noted that the predictor extension introduced in this section is based on control considerations. Thus, there is a substantial difference in the predictor concept when compared with the usually applied predictors with circular flightpath continuation which are based on geometric/kinematic relations alone.

With reference to equations (4) and (13), the predictor transfer function for the control related flightpath continuation can be expressed as

$$Y_{PR} = \frac{e_{PR}(s)}{\Delta\dot{\gamma}(s)} = K_{PR} V \frac{(\overline{T}_{PR}^2/2)s^2 + T_{PR}s + 1}{s^2} \tag{14}$$

Combining equations (9b) and (14) yields the open-loop transfer function for the effective predictor to longitudinal control response:

$$\frac{e_{PR}(s)}{\delta_e(s)} = K_C^* \frac{s^2 + 2(T_{PR}/\overline{T}_{PR}^2)s + 2/\overline{T}_{PR}^2}{s^2(s^2 + 2\zeta_{SP}\omega_{SP}s + \omega_{SP}^2)} \tag{15}$$

where

$$K_C^* = -K_{PR} Z_\alpha M_{\delta_e} \overline{T}_{PR}^2/2 \tag{16}$$

From equation (15) it follows that, by proper selection of $\overline{T}_{PR}$ and the prediction time T_{PR}, the desired K/s characteristic in the frequency region of pilot–predictor–vehicle system crossover can be achieved. For this purpose, the relation

$$\overline{T}_{PR} \ll T_{PR} \tag{17}$$

may be selected. Then, the zeros of the numerator which may be rewritten as

$$s^2 + 2\frac{T_{PR}}{\overline{T}_{PR}^2}s + \frac{2}{\overline{T}_{PR}^2} = \left(s + \frac{1}{T_1}\right)\left(s + \frac{1}{T_2}\right) \tag{18}$$

can be approximated by

$$T_1 \approx T_{PR}, \qquad T_2 \approx \frac{\overline{T}_{PR}^2}{2T_{PR}} \tag{19}$$

The predictor–aircraft transfer characteristics for the extended predictor are illustrated in Fig. 6. There is a K/s characteristic in the frequency region between $1/T_1$ and $1/T_2$. By proper selection of T_{PR} and $\overline{T}_{PR}$ according to equation (19), it is possible to place $1/T_2$ close to ω_{SP}.

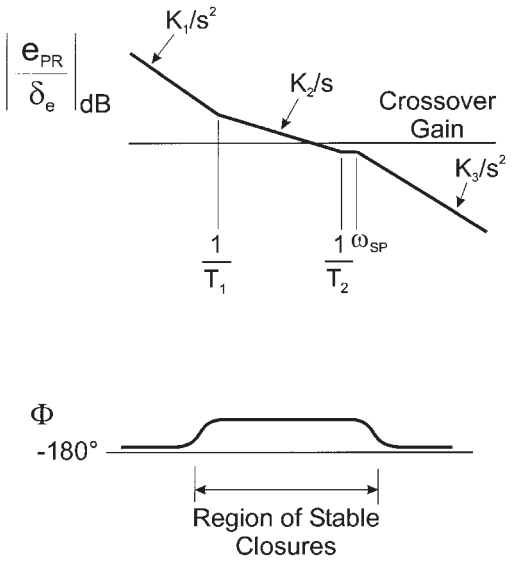

Fig. 6 Asymptotic Bode plot for the predictor–aircraft system (predictor extension, control related flightpath continuation)

Thus, a K/s characteristic can be achieved which practically extends from $1/T_1$ to ω_{SP}. This is the frequency region where pilot–system crossover is possible.

From the preceding considerations it follows as a general characteristic that the K/s frequency region is set by $1/T_1$ and ω_{SP}: the length of the K/s frequency region decreases with a decrease in the difference between $1/T_1$ and ω_{SP} and vice versa. This is a basic result according to which $1/T_1$ may be selected with reference to ω_{SP} in order to yield an appropriately large K/s frequency region. Because of $T_1 \approx T_{PR}$, the required T_1 value is achieved by proper selection of the prediction time T_{PR}.

With regard to aircraft dynamics, the short period frequency ω_{SP} is a key aircraft factor for the K/s frequency region. It may be noted in this context that ω_{SP} is a significant flying quality metric for which an acceptable range is specified [**14**, **15**].

The following example is considered to provide an insight into the numerical magnitude of T_{PR} and $\overline{T}_{PR}$ for achieving a K/s frequency region of proper length. A short period frequency range $\omega_{SP} \geqslant 2.0\,\text{rad/s}$ is assumed which can be regarded as covering a wide range of values possible with aircraft. Furthermore, achieving one decade of K/s frequency region is considered a reasonable objective. With reference to equation (19), T_{PR} and $\overline{T}_{PR}$ may then be selected as $T_{PR} \approx 5.0$ s and $\overline{T}_{PR} \approx 2.2$ s.

The pilot gain for loop closure can be determined with the crossover condition

$$|Y_P Y_{PR} Y_C|_{s=i\omega_C} = 1 \tag{20}$$

According to the crossover model [**11**], the dynamic behaviour of the pilot can be described with the following relation if there is a K/s characteristic of the predictor–aircraft system in the frequency region around crossover:

$$Y_P(s) = K_P e^{-\tau_e s} \tag{21}$$

Thus, the crossover condition, equation (20), yields

$$\left| K_P e^{-\tau_e s} K_C^* \frac{(s + 1/T_1)(s + 1/T_2)}{s^2(s^2 + 2\zeta_{SP}\omega_{SP}s + \omega_{SP}^2)} \right|_{s=i\omega_C} = 1 \tag{22}$$

For

$$1/T_1 \ll \omega_C, \qquad \omega_C \ll \omega_{SP}, \qquad 1/T_2 \approx \omega_{SP} \tag{23}$$

the following result for the pilot gain holds:

$$K_P \approx \frac{\omega_{SP}\omega_C}{K_C^*} \tag{24}$$

Summing up the foregoing considerations, the goal of a K/s frequency region centred around pilot–system crossover can be achieved with the predictor extension introduced in this section. Thus, the controlled predictor–

aircraft element represents a system requiring minimum pilot compensation.

5 SYSTEM STABILITY AND BANDWIDTH

Closed-loop stability is evaluated with the root locus technique, yielding results of a rather general nature.

The stability characteristics of the basic predictor with circular flightpath continuation are illustrated in Fig. 7 which shows the root locus for the pilot–predictor–aircraft system. The dynamic behaviour of the pilot in the case of the basic predictor can be described with a model adopting a very low-frequency lag equalization. Accordingly,

$$Y_P(s) = K_P \frac{e^{-\tau_e s}}{T_I s + 1} \tag{25}$$

For the frequency region in mind, the delay can be incorporated into the root locus diagram using the approximation $e^{-\tau_e s} \approx (1 - \tau_e/2)/(1 + \tau_e/2)$.

Figure 7 shows that there are three root locus branches. One branch emerges from the short period poles (closed-loop attitude mode) and another from the origin (closed-loop path mode). The third branch is introduced by the low-frequency lag of the pilot. The path mode is basically fixed by the predictor numerator zeros ($\omega_{PR} = \sqrt{2}/T_{PR}$, $\zeta_{PR} = 1/\sqrt{2}$). There is a significant destabilization of the attitude mode. Further, its frequency is considerably decreased in the first part of the root locus branch.

The stability characteristics of the predictor extension with control related flightpath continuation are illustrated in Fig. 8. This figure shows that there are two root locus branches, yielding closed-loop attitude and path modes. The low-frequency path mode emerging from the origin profits from loop closure since the increase in pilot gain significantly contributes to damping and frequency. The attitude mode shows a decrease in damping.

Comparing the predictor candidates (Figs 7 and 8), the predictor extension with control related flightpath continuation shows the following advantages in closed-loop stability:

(a) improved stability of the closed-loop path mode (higher damping, greater natural frequency),
(b) less destabilization of the closed-loop attitude mode (less reduction in damping, practically no decrease in frequency),
(c) the path mode profits more from destabilization of the attitude mode (because of zero configuration).

For the predictor extension with control related flightpath continuation, some closed-loop stability properties are described in the following. The root locus presented in Fig. 8 shows that the closed-loop system is stable for gain values of practical interest. This result is supported by an analytical solution for the pilot gain $K_{P_{crit}}$ at the stability boundary. A simplified treatment for determining $K_{P_{crit}}$ is applied where the stability conditions are evaluated using a pilot model which is represented by a pure gain without time delay ($Y_P = K_P$). The following result is obtained for the pilot gain necessary for stability:

$$K_P < K_{P_{crit}} \tag{26a}$$

where

$$K_{P_{crit}} \approx \frac{2\zeta_{SP}}{1 - 2\zeta_{SP}} \frac{\omega_{SP}^2}{K_C^*} \tag{26b}$$

This expression shows that $\overline{T}_{PR}$ has a strong effect (because

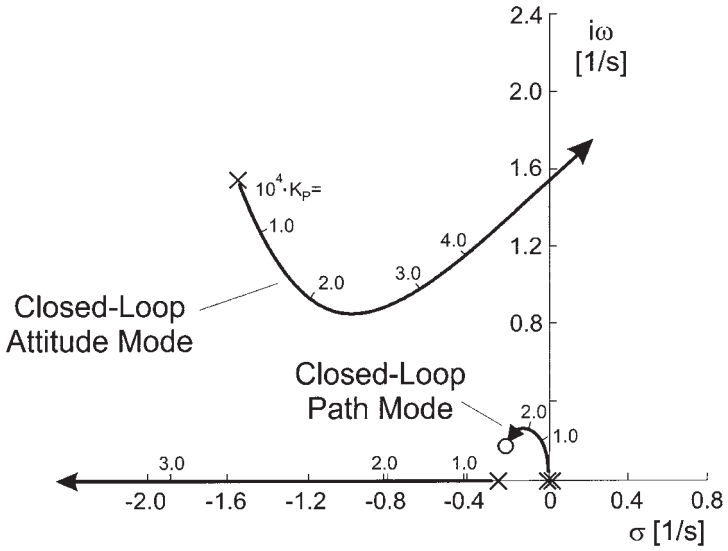

Fig. 7 Root locus of the closed-loop system with basic predictor with circular flightpath continuation: $T_{PR} = 5.0$ s, $K_{PR} = 1.0$, K_P in rad/m

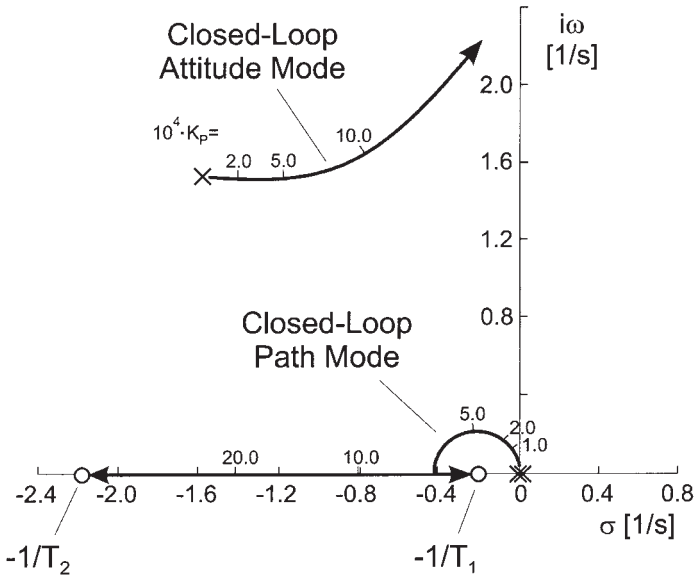

Fig. 8 Root locus of the closed-loop system with predictor extension with control related flightpath continuation: $1/T_2 = \omega_{SP}$, pilot model [equation (23)] with $\tau_e = 0.25$ s, $T_{PR} = 5.0$ s, $K_{PR} = 1.0$, K_P in rad/m

of $K_C^* = -K_{PR} Z_\alpha M_{\delta_e} \overline{T}_{PR}^2/2$). Further, the damping ratio ζ_{SP} of the open-loop short period mode is significant for closed-loop stability. From equation (26b) it follows that there is no closed-loop instability if

$$\zeta_{SP} > \zeta_{SP_{crit}}$$

where

$$\zeta_{SP_{crit}} = 0.5$$

However, closed-loop stability is practically assured also for smaller ζ_{SP} values if they belong to the range $\zeta_{SP} > 0.35$ which is acceptable from a flying quality standpoint [**14**, **15**]. This is because the pilot gain for crossover is significantly smaller than $K_{P_{crit}}$. The following relation obtained from equations (24) and (26b)

$$\frac{K_P}{K_{P_{crit}}} \approx \frac{1 - 2\zeta_{SP}}{2\zeta_{SP}} \frac{\omega_C}{\omega_{SP}} \tag{27}$$

shows that practically $K_P/K_{P_{crit}} \ll 1$ for $\omega_C/\omega_{SP} < 1$ and $0.35 < \zeta_{SP} < \zeta_{SP_{crit}}$. These analytical solutions are supported by results from simulation experiments for the pilot gain at crossover.

System bandwidth concerns command following and disturbance regulation. Basically, the low-frequency path mode is significant for the maximum achievable closed-loop system bandwidth in both predictor candidate cases.

For the basic predictor with circular flightpath continuation, the root locus presented in Fig. 7 shows that the frequency of the path mode is closely related to the zeros of the predictor transfer function numerator. Thus, the numerator zeros have a primary impact on the achievable closed-loop system bandwidth. The relation for the natural frequency of the numerator may serve as an estimate:

$$\omega_{PR} = \frac{\sqrt{2}}{T_{PR}}$$

The predictor extension with control related flightpath continuation has potential for an improvement in closed-loop system bandwidth. This is because the path mode has a greater natural frequency. The root locus depicted in Fig. 8 shows that bandwidth profits from loop closure because the frequency of the path mode increases with pilot gain for the range of practically interesting values. An indication for system bandwidth is provided by the following relations for the closed-loop path mode roots, ω'_P and ζ'_P, which can be derived with the use of the pilot gain described by equation (24):

$$\omega'_P \approx \sqrt{\frac{\omega_C/T_{PR}}{1 + \omega_C/\omega_{SP}}}, \qquad \zeta'_P \omega'_P \approx \frac{\omega_C/2}{1 + \omega_C/\omega_{SP}} \tag{28}$$

6 EXPERIMENTAL VERIFICATION

The compensatory control issues considered in the previous sections were the subject of an experimental verification in a simulation test program. Emphasis is placed on the predictor extension because of its superior dynamic properties.

Five pilots with different professional background (airline pilots, private pilot) performed the simulation experi-

ments. A fixed-base simulator was used which was equipped with a predictive flightpath display, the layout of which is shown in Fig. 1. The non-linear six-degree-of-freedom aircraft model used in the simulation experiments can be regarded as representative of small twin jet engine aircraft. The flight tasks consisted of following a trajectory with alternating descending and ascending segments.

A basic issue for the experimental verification is the prediction time T_{PR} because it is a factor of primary concern for achieving a K/s frequency region that is broad enough and, thus, has a substantial effect on compensatory control characteristics and on related pilot performance. Results of the simulation experiments for the control of the predictor position are presented in Fig. 9 (box plot technique, 95 per cent confidence interval). As a basic result, the predictor position is effectively controlled by the pilots, showing rather small deviations from the command flightpath. The pilot ratings are favourable and in support of the concept of the perspective flightpath display with the predictor as an efficient means for improving aircraft guidance and control. Furthermore, Fig. 9 shows that there is a significant effect of the prediction time T_{PR}, yielding a decrease in the predictor position error with a decrease in T_{PR}, and vice versa.

Results for the control activity of the pilots are presented in Fig. 10 which shows the elevator deflections for minimizing the predictor position errors. The effect of the prediction time T_{PR} manifests in an increase in control activity with a decrease in T_{PR}.

The predictor, the original purpose of which is to control the future position at the prediction time ahead, is also an efficient means of controlling the current position of the aircraft. Results of the simulation experiments in Fig. 11 show that the current position is effectively controlled. Furthermore, there is some effect of the prediction time

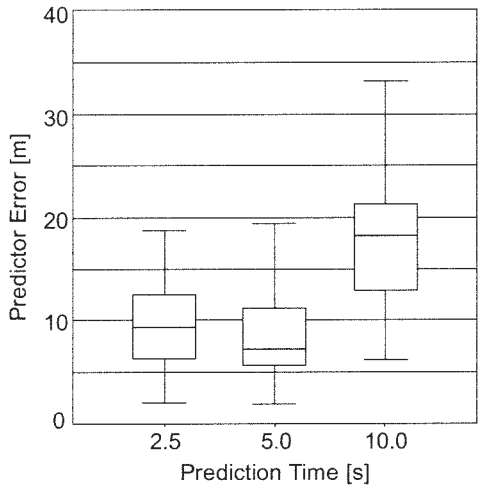

Fig. 9 Deviation of the predictor position (predictor extension with control related flightpath continuation)

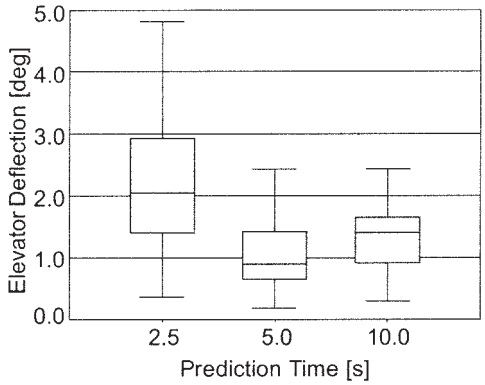

Fig. 10 Pilot control activity (predictor extension with control related flightpath continuation)

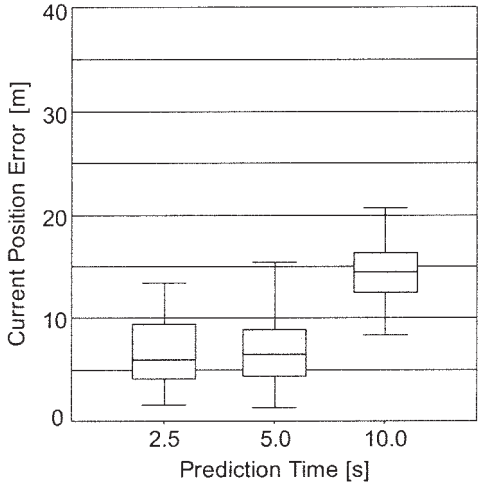

Fig. 11 Deviation of the current position (predictor extension with control related flightpath continuation)

T_{PR}, which is reduced when compared with the predictor error case.

The result indicating that there is an increase in control activity with a decrease in T_{PR} can be explained with pilot loop closure behaviour. This effect is illustrated in Fig. 12 which schematically shows frequency responses for two numerator zeros, $1/T_{1,a}$ and $1/T_{1,b}$. An increase from $1/T_{1,a}$ to $1/T_{1,b}$ is considered which is due to a decrease in the prediction time from $T_{PR,a}$ to $T_{PR,b}$ (since $T_{1,a} \approx T_{PR,a}$ and $T_{1,b} \approx T_{PR,b}$). As a consequence of the increase from $1/T_{1,a}$ to $1/T_{1,b}$, the K/s frequency region now begins at a higher frequency and is shifted downwards (dashed line). Thus, there is a decrease in the gain in the K/s frequency region. From Fig. 12 it follows that the gain decrease in the K/s frequency region from K_a to K_b may be approximated by

$$\frac{K_b}{K_a} \approx \frac{T_{1,b}}{T_{1,a}} \approx \frac{T_{PR,b}}{T_{PR,a}} \tag{29}$$

The downward shift of the K/s characteristic requires an

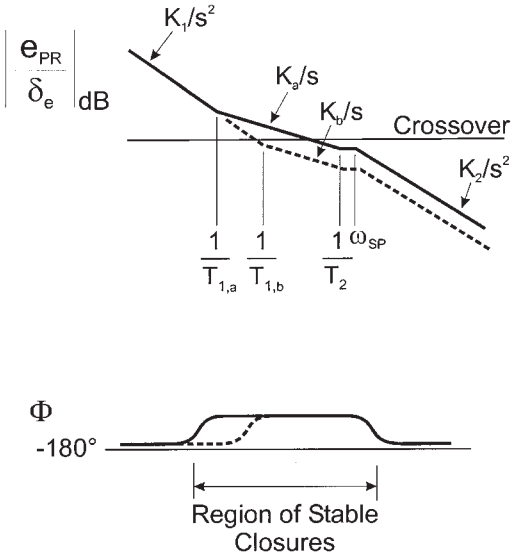

Fig. 12 Effect of the prediction time on frequency responses (predictor extension with control related flightpath continuation)

increase in pilot gain for loop closure from $K_{P,a}$ to $K_{P,b}$ which is approximately the inverse of the ratio expressed in equation (29):

$$\frac{K_{P,b}}{K_{P,a}} \approx \frac{T_{PR,a}}{T_{PR,b}} \tag{30}$$

The described results are supported by an evaluation of simulation experiments (Fig. 13). This figure shows frequency responses for two prediction times, $T_{PR} = 2.5$ s and $T_{PR} = 5.0$ s, and corresponding pilot gains estimated from the simulation experiments. The change in the gains compares well with the above considerations, including equation (30). Furthermore, the results presented in Fig. 13 confirm that pilot–system crossover is in the K/s region. They also show that it is near the frequency for maximum phase margin.

7 POSSIBLE CONTROL PROBLEM RELATED TO LONG-TERM DYNAMICS

There is a general long-term dynamics problem in manual or automatic flightpath control for aircraft that operate on what is commonly referred to as the reverse of the power-required versus speed curve. This problem concerns a closed-loop instability of the pilot–aircraft system when the usual piloting technique to adjust flightpath with pitch attitude by the use of pitch control only is applied (throttle setting not changed by the pilot) [**14**, **15**]. Such a long-term stability problem may also exist with a predictor-based control of the flightpath. For considering this issue, the aircraft model has to be supplemented to include long-term dynamics effects.

The long-term dynamics effects in mind can be described with an aircraft model accounting for the phugoid and short period mode (characterized by ω_P, ζ_P and ω_{SP}, ζ_{SP}) and the low-frequency numerator zero $1/T_{h_1}$. The corresponding transfer function reads (e.g. according to reference [**13**])

$$Y_C = \frac{\Delta\dot{\gamma}(s)}{\delta_e(s)} = -\frac{Z_\alpha M_{\delta_e}}{V} \frac{s(s + 1/T_{h_1})}{(s^2 + 2\zeta_{SP}\omega_{SP}s + \omega_{SP}^2)(s^2 + 2\zeta_P\omega_P s + \omega_P^2)} \tag{31}$$

With the predictor extension model equation (14) and the numerator zeros expression equation (18), the relation for the predictor–aircraft system can be written as

$$\frac{e_{PR}(s)}{\delta_e(s)} = K_C^* \frac{(s + 1/T_{h_1})(s + 1/T_1)(s + 1/T_2)}{s(s^2 + 2\zeta_{SP}\omega_{SP}s + \omega_{SP}^2)(s^2 + 2\zeta_P\omega_P s + \omega_P^2)} \tag{32}$$

The long-term stability problem in mind is graphically illustrated in Fig. 14 which shows the root locus for the pilot–predictor–aircraft system. The stability problem specifically relates to the root locus branch between the origin and the numerator zero $1/T_{h_1}$, representing an aperiodic low-frequency mode of motion. Figure 14 reveals that stability or instability of this mode is determined by the sign of the numerator zero $1/T_{h_1}$. The closed-loop system is stable provided that $1/T_{h_1} > 0$ (upper part of Fig. 14), and instability is introduced if $1/T_{h_1} < 0$ (lower part of Fig. 14). This result can be attributed to thrust and drag characteristics of the aircraft according to the following analytical solution:

$$\frac{1}{T_{h_1}} \approx 2\frac{g}{V}\left[\left(1 - \frac{1}{2}\frac{V}{T}\frac{\partial T}{\partial V}\right)\frac{C_D}{C_L} - \frac{\partial C_D}{\partial C_L}\right] \tag{33}$$

The bracketed term in equation (33) is a measure for what is called front side or reverse of the power-required curve. Accordingly, the following relations hold:

$1/T_{h_1} > 0$: operation on the front side of the power-required curve, equivalent to closed-loop long-term stability;

$1/T_{h_1} < 0$: operation on the reverse of the power-required curve, equivalent to closed-loop long-term instability.

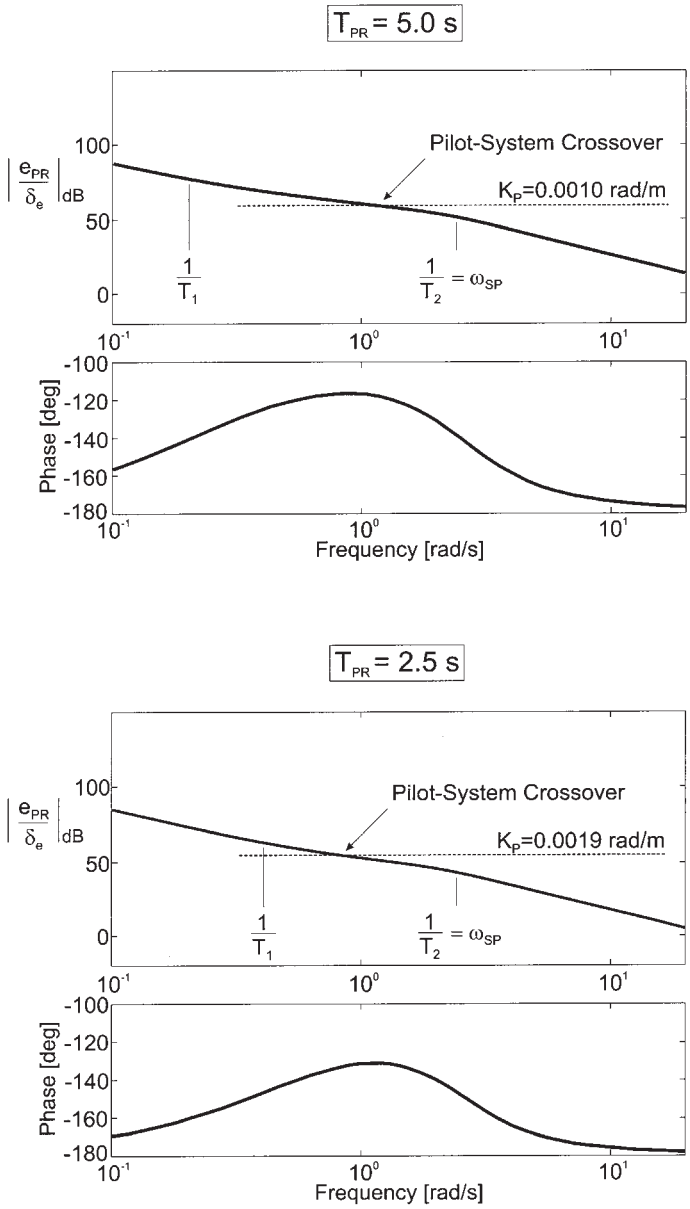

Fig. 13 Effect of the prediction time on frequency responses (predictor extension with control related flightpath continuation, $T_1 \approx T_{\mathrm{PR}}$, $K_{\mathrm{PR}} = 1.0$)

Further, it may be noted in Fig. 14 that there are only minor effects on the other root locus branches when compared with the case shown in Fig. 8. The phugoid poles cause some change which only concerns small pilot gains. The change tends to disappear for higher gains. The closed-loop attitude mode emerging from the short period poles shows practically no change.

With regard to the characteristics in the K/s frequency region, there are basically no changes. The K/s characteristic is determined by the short-term model of aircraft dynamics, equation (9b). Thus, it is confirmed that the considerations using the short-term dynamics model adequately describe the properties in the crossover frequency region.

The addressed long-term instability can be removed by well-known means [**13**, **16**]. The basic physical reason underlying this stabilizing means is that a negative change in thrust with speed $\partial T/\partial V < 0$ is introduced to change $1/T_{h_1}$ from the unstable to the stable region. This effect is indicated in equation (33) by the term $\partial T/\partial V$. Such a thrust change may be produced artificially by a control system (autothrottle) or by the pilot with coordinated control actions of thrust and elevator.

8 CONCLUSIONS

The guidance and control enhancement possible with perspective flightpath displays with a predictor has been

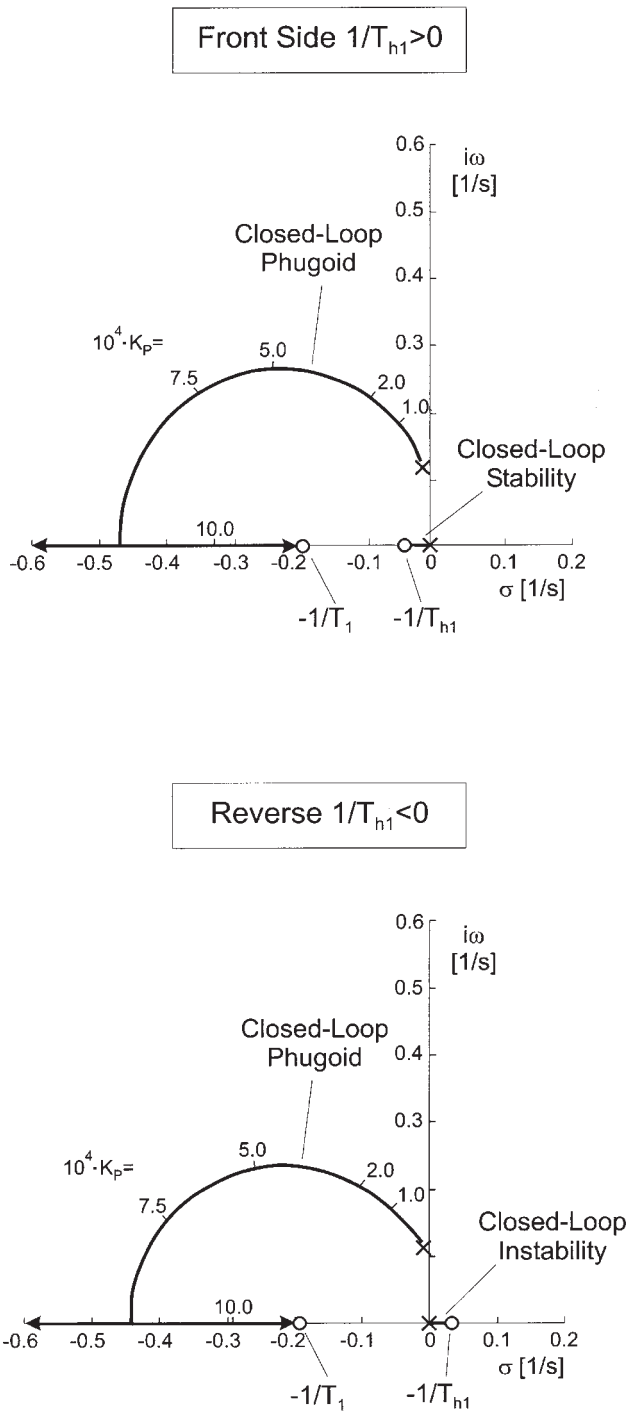

Fig. 14 Root locus of the closed-loop system for long-term dynamics: $1/T_2 = \omega_{SP}$, pilot model [equation (23)] with $\tau_e = 0.25$ s, $T_{PR} = 5.0$ s, $K_{PR} = 1.0$, K_P in rad/m

considered for an application to the longitudinal motion. This display type provides the pilot with command and status information in a three-dimensional format. Pilot-centred requirements for compensatory control have been considered for achieving maximum performance of the closed-loop pilot–predictor–aircraft system with minimum pilot effort. Two predictor candidates for this primary goal have been dealt with, yielding the following properties: a transfer characteristic that is approximately a pure gain and another one that approximates a pure integration over an adequately broad frequency region centred around pilot–system crossover. The pure gain transfer characteristic can be attained with the usual predictor type which is based on geometric/kinematic relations (circular flightpath continuation). The pure integration transfer characteristic, which has superior properties, can be achieved with a predictor extension that is based on control considerations. Thus, a conceptual design element has been introduced that yields a substantial difference from the usually applied predictor. Key configuration factors of the pilot–predictor–aircraft system have been identified and optimized. The conceptual and theoretical control issues have been the subject of a simulation test program. The results indicate that the predictor is an efficient means of compensatory flightpath control.

REFERENCES

1 **Theunissen, E.** Integrated design of a man–machine interface for 4-D navigation. PhD dissertation, TU Delft, The Netherlands, 1997.

2 **Theunissen, E.** and **Mulder, M.** Availability and use of information in perspective flightpath displays. In Proceedings of AIAA Flight Simulation Technologies Conference, 1995, pp. 137–147.

3 **Grunwald, A. J.** Improved tunnel display for curved trajectory following: control considerations. *J. Guidance, Control, and Dynamics*, 1996, **19**(2), 370–377.

4 **Grunwald, A. J.** Improved tunnel display for curved trajectory following: experimental evaluation. *J. Guidance, Control, and Dynamics*, 1996, **19**(2), 378–384.

5 **Haskell, I. D.** and **Wickens, C. D.** Two- and three-dimensional displays for aviation: a theoretical and empirical comparison. *Int. J. Aviat. Psychol.*, 1993, **3**(2), 87–109.

6 **Wickens, C. D., Fadden, S., Merwin, D.** and **Ververs, P. M.** Cognitive factors in aviation display design. In Proceedings of 17th AIAA/IEEE/SAE Digital Avionics Systems Conference, Bellevue, WA, 31 October–6 November 1998.

7 **Funabiki, K., Muraoka, K., Terui, Y., Harigae, M.** and **Ono, T.** In-flight evaluation of tunnel-in-the sky display and curved approach pattern. In AIAA Guidance, Navigation, and Control Conference Proceedings, 1999, pp. 108–114.

8 **Sachs, G.** and **Möller, H.** Synthetic vision flight tests for precision approach and landing. In AIAA Guidance, Navigation, and Control Conference Proceedings, 1995, pp. 1459–1466.

9 **Sachs, G., Dobler, K.** and **Hermle, P.** Flight testing synthetic vision for precise guidance close to the ground. In AIAA Guidance, Navigation, and Control Conference Proceedings, 1997, pp. 1210–1219.

10 **Sachs, G.** Perspective flightpath predictor for minimum pilot compensation. *Aerospace Sci. and Technol.*, 1999, **3**(4).

11 **McRuer, D. T.** Pilot modeling. AGARD-LS-157, 1988, pp. 2-1–2-30.

12 Hess, R. A. Feedback control models—manual control and tracking. In *Handbook of Human Factors and Ergonomics*, 2nd edition, 1997, pp. 1249–1294 (John Wiley, New York).
13 McRuer, D. T., Ashkenas, I. and **Graham, D.** *Aircraft Dynamics and Automatic Control*, 1990 (Princeton University Press, Princeton, New Jersey).
14 Flying qualities of piloted airplanes. MIL-F-8785C, 1991.
15 Flying qualities of piloted aircraft. MIL-STD-1797, 1990.
16 Brockhaus, R. *Flugregelung*, 1994 (Springer-Verlag, Berlin).